Nano-precipitation-strengthened steels

M.C. Niu[a,b], H.J. Kong[c], B.C. Zhou[a,b], W. Wang[d,*], Z.B. Jiao[a,b,*]

[a] *Department of Mechanical Engineering, The Hong Kong Polytechnic University, Hong Kong, China*
[b] *The Hong Kong Polytechnic University Shenzhen Research Institute, Shenzhen 518057, China*
[b] *Department of Mechanical Engineering, City University of Hong Kong, Hong Kong, China*
[d] *Shi-changxu Innovation Center for Advanced Materials, Institute of Metal Research, Chinese Academy of Sciences, Shenyang 110016, China*
* *Corresponding authors: wangw@imr.ac.cn; zb.jiao@polyu.edu.hk*

1. Introduction

Ultra-high strength steels (UHSSs) generally refer to steels with yield strength (YS) greater than 1380 MPa (200 ksi) [1]. In the mid-1940s, the U.S. Navy firstly developed UHSSs with high strength, good toughness, and high weldability to replace the conventional steels [2,3] Over the years, UHSSs have been widely used in mining, metallurgy, machinery manufacturing, power generation, marine engineering, aerospace, and other industrial fields. UHSSs have been the preferred materials for energy saving and emission reduction, as well as the lightweight design of structual components. However, most conventional UHSSs are developed in martensitic and bainitic steels with a high carbon content or high alloy additions, which leads to many problems, including low ductility and toughness, poor weldability, high production cost, and limited fabrication sizes [4-6]. Hence, it is urgent to develop advanced UHSSs with excellent mechanical and metallurgical properties and low cost. Precipitation strengthening is an effective method to improve the mechanical properties of steels, and many studies reveal that nanoscale precipitation can provide steels with an extremely high strengthening response [7,8]. So far various classes of nano-precipitation-strengthened steels have been developed, such as high-strength low-alloy (HSLA) steels, low-carbon precipitation-hardened (PH) stainless steels, and maraging steels [9-12]. In this chapter, we highlight recent advances in nano-precipitation-strengthened steels. Special attention is placed on the precipitation mechanisms of and the correlation between the precipitate microstructure and bulk alloy properties, including tensile, creep, corrosion, and welding properties. In addition, the

opportunities and challenges of nano-precipitates-strengthened steels in engineering applications are discussed.

2. Nanoscale precipitates in steels

2.1 Ni_3Ti precipitate

Ni_3Ti is an important strengthening phase in Fe-Ni-Ti and Fe-Mn-Ni-Ti steels. The crystal structure of η-Ni_3Ti is shown in **Fig. 1**a. The η-Ni_3Ti phase has a hexagonal structure (a = 0.5093 nm and c = 0.8306 nm) with a rod-like morphology [13]. The orientation relationship between the Ni_3Ti precipitates and body-centered cubic (bcc) matrix is $\{011\}_\alpha//\{0001\}_\eta$ and $< 11\bar{1} >_\alpha//< 11\bar{2}0 >_\eta$ [13]. Because the Ni_3Ti precipitates are semi-coherent with the bcc matrix, the interface energy required for nucleation is high. Therefore, the η-Ni_3Ti precipitates tend to nucleate inhomogeneously at the crystal defects, such as dislocations and grain and lath boundaries. Kim *et al.* [14] reported that Ni_3Ti precipitates at grain boundaries were one of the important reasons causing severe grain-boundary embrittlement of Ni_3Ti-strengthened steels after isothermal aging. Some studies found that alloying of some elements has a positive inhibitory effect on the brittle intergranular failure of maraging steels. For example, Heo *et al.* [15] reported that the Mo addition can prevent the premature brittle intergranular failure of a Fe-Ni-Mn-Ti alloy due to the enhancement of grain boundary strength by the Mo segregation at grain boundaries. In addition, other elements, such as Co, Cr, W, Si, and B are also added to reduce the grain-boundary embrittlement of Ni_3Ti-strengthened steels [15-17].

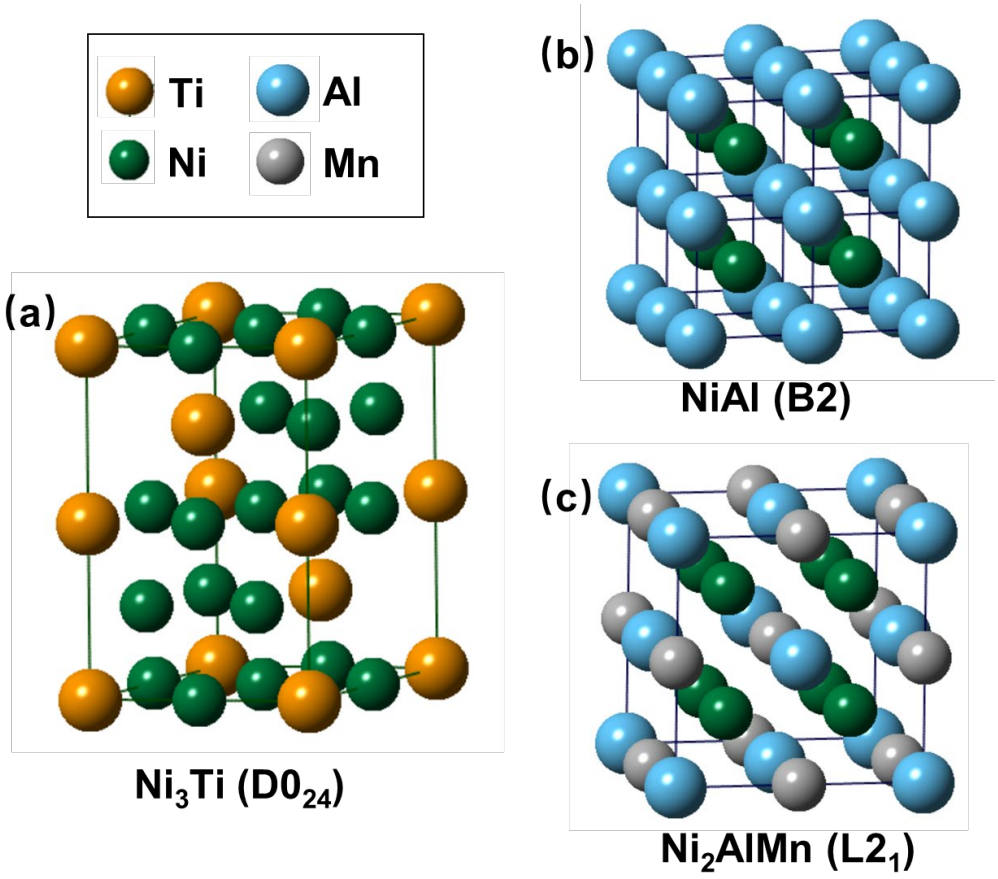

Figure 1. Crystal structures of (a) Ni_3Ti, (b) NiAl, and (c) Ni_2AlMn.

2.2 NiAl precipitate

NiAl precipitates have been widely used in the UHSSs, such as maraging steels, HSLA steels, and ferritic heat-resistant steels [18,19]. The crystal structure of NiAl phase is shown in **Fig. 1**b. NiAl has a B2 crystal structure, where Al occupies the body-center sites and Ni occupies the cube-corner sites. The lattice constant of NiAl is 0.2887 nm, which is close to that of bcc Fe (0.2866 nm) [20,21]. NiAl precipitates have a super strengthening effect because of its high order energy. However, the steels strengthened by NiAl precipitates often have a low ductility (less than 5% uniform elongation), which seriously limits their engineering applications [22]. Recently, remarkable progress has been made in the development of NiAl-strengthened steels. For example, a low Ni steel with a yield strength of 1.3 GPa and a satisfactory elongation of 10% was developed through precisel optimizing the alloy composition and controlling the precipitate microstructure [20]. Jiang *et al.* [23] designed novel economical UHSSs with a yield strength of 2 GPa with a considerable ductility. The NiAl

precipitates in these steels have an extremely low lattice misfit, which decreases the nucleation energy and results in a high number density (10^{24} m^{-3}) of precipitates. This low misfit between the precipitates and matrix also decreases the contribution of dislocation interaction; hence, the ductility is not significantly sacrificed. In addition, Mo was found to be rejected from NiAl precipitates and accumulated at the interface, retarding the coarsening of the NiAl precipitates.

2.3 Cu precipitate

Many studies on the precipitation behavior of the Cu-rich precipitates in martensitic/ferritic steels have been carried out. Heo *et al.* [24] studied the phase transformation of Cu precipitates in an Fe–3Si–2Cu steel during aging by using transmission electron microscopy (TEM). The transformation sequences of Cu precipitates in the bcc matrix are displayed in **Fig. 2**. In the early stages, the Cu precipitates of 3 ~ 5-nm-sized have a bcc structure, which are coherent with the ferrite matrix. Then, the bcc Cu precipitates gradually transform to 9R with a twinned close-packed structure. Subsequently, the 9R precipitates transform into twinned face-centered-cubic (fcc) Cu and finally transform into stable fcc Cu after a long aging time. Han *et al.* [25] reported that the maximum strengthening effect is attributed to the bcc Cu precipitates. The strengthening effect is almost completely lost, when the structure transforms to fcc. Generally, Cu precipitates have a weak strengthening effect; hence, they usually combine with other hard precipitates, such as NiAl and Ni_3Ti, to get a high strengthening effect. Kapoor *et al.* [26] and Jiao *et al.* [27] reported two types of co-precipitation processes of Cu and NiAl precipitates in the Fe–Cu–Ni–Al-based steels, and schematically illustrated in **Fig. 3** [27]. One is the homogeneous precipitation of Cu, followed by the heterogeneous precipitation of NiAl at the Cu/matrix interface, because the first formation of Cu precipitates provides heterogeneous nucleation sites for the precipitation of NiAl in the steels with high Cu/Al and Cu/Ni radios. The other is the homogeneous precipitation of NiAl, followed by the heterogeneous precipitation of Cu. In this case, the first formation of NiAl precipitates leads to the rejection of Cu outward to the NiAl precipitates in the steels with low Cu/Al and Cu/Ni radios [27]. The unique coexistence of the two precipitation pathways and the co-precipitation effect significantly accelerate the age hardening

kinetics and ultimately enhance the hardening response. Schnitzer *et al.* [28] investigated the synergistic precipitation effects of Ni_3Ti, NiAl, and Cu precipitates in an Fe–Cr–Ni–Ti–Al-Cu steel. They found that the effect of Cu on the nucleation of NiAl and Ni_3Ti precipitates was different. On the one hand, the partition of Cu in the NiAl precipitate reduces the activation energy by reducing the lattice misfit between the matrix and NiAl precipitates; on the other hand, the formation of Cu precipitates acts as a nucleation site for the precipitation of Ni_3Ti [28]. Both effects caused by Cu additions accelerate the precipitation in the steel.

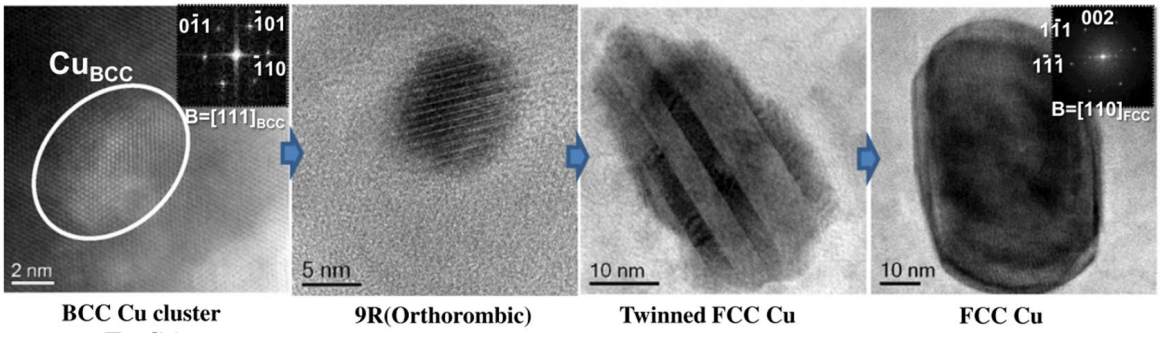

Figure 2. The transformation sequences of Cu precipitates in the bcc Fe matrix [24].

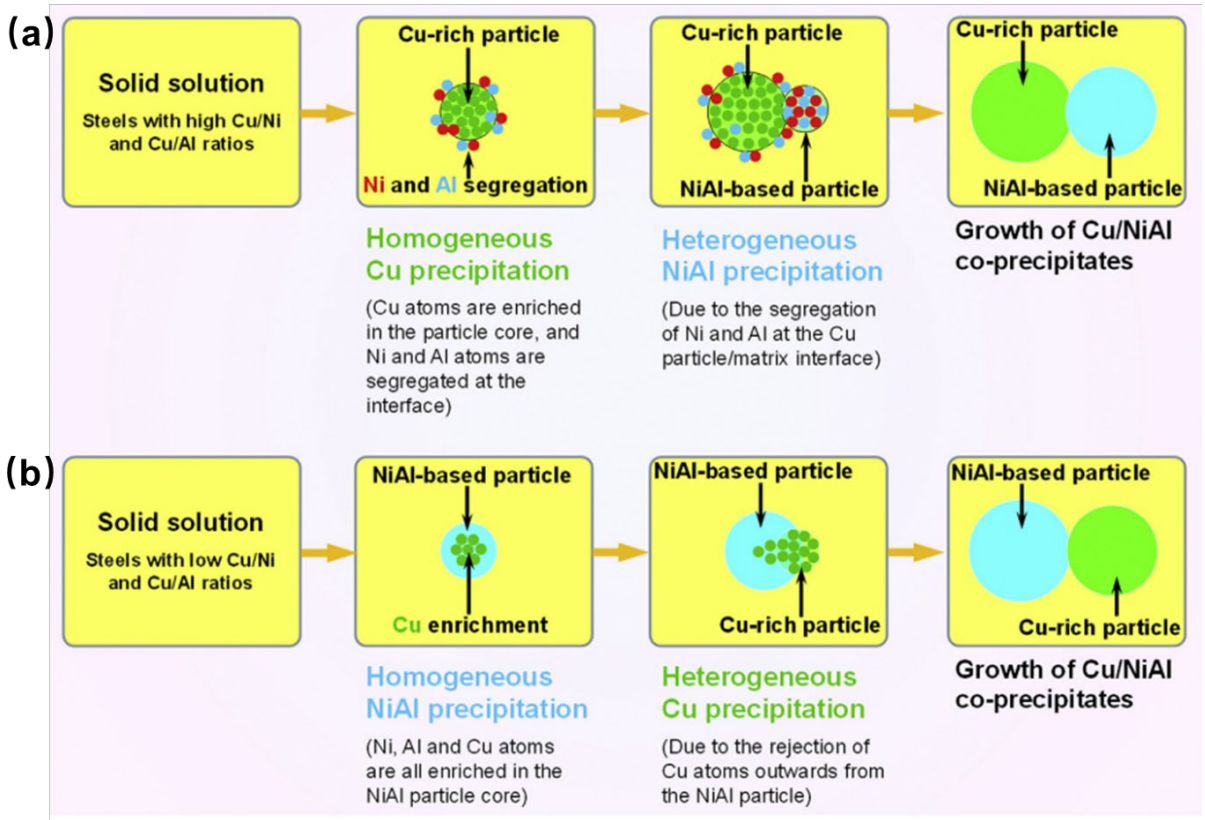

Figure 3. Co-precipitation of Cu and NiAl precipitates in the Fe–Cu–Ni–Al-based steels: (a) steels with high

Cu/Ni and Cu/Al radios steels and (b) steels with high Cu/Ni and Cu/Al radios [27].

2.4 Ni_2AlMn precipitate

The UHSSs strengthened by NiAl or Ni_3Ti precipitates require a large amount of Ni additions, which causes an extremely high cost. In recent years, a kind of lean Fe-Ni-Al-Mn-based steels strengthened by high number densities of Heusler Ni_2AlMn precipitates was developed. As shown in **Figure 1**c, the Ni_2AlMn phase has an order $L2_1$ crystal structure with a lattice constant of 0.5824 nm [29]. Previous studies indicated that the precipitation behavior of Ni_2AlMn is highly sensitive to the alloy composition [30-32]. For example, Millán *et al.* [31] designed an Fe-Mn-Ni-Al UHSS with a low Ni content (5 at.%). The combined TEM and APT results reveal that the Al alloying is beneficial to the formation of B2-Ni(Mn,Al) precipitates, in which a small amount of Mn partitions to the NiAl precipitate by occupying the Al sublattice. High Al alloying promotes the formation of Ni_2MnAl precipitates, whereas medium Al alloying can induce the precipitation of both Ni(Mn,Al) and Ni_2MnAl precipitates. Jiao *et al.* [30] studied the effect of Mn additions on the precipitation behavior of the Fe-5Ni-1Al-*x*Mn (*x* = 0, 1, 3, and 5 wt.%) steels. The atom probe tomography (APT) results are displayed in **Fig. 4**. Ni(Al,Mn) precipitates are detected in the low Mn steels (0 ~ 3 at.%), whereas the co-precipitation of fine Ni(Al,Mn) and coarse Ni_2AlMn precipitates are observed in the high Mn steel (5 at.%). It indicates that the Ni_2AlMn precipitates are transformed from the Ni(Al,Mn) precipitates. The tensile results show that the ductility of the steels drops with the increased Mn content, which indicates that the fine-scale dispersed Ni(Al,Mn) precipitates can cause a significant increase in strength while remaining a decent ductility, whereas the coarse Ni_2AlMn precipitates generally cause an increase in strength but a loss in the ductility. Heo *et al.* [33] studied the effect of Al on the mechanical properties of Fe-Ni-Mn-Al alloys. The precipitation of Ni_2AlMn can suppress the formation of MnNi precipitates at grain boundaries. Hence, the fracture mode changes from intergranular to transgranular cleavage fracture. Further increasing the content of Al to 4.2 wt.% results in a discontinuous growth of Ni_2MnAl precipitates in the

steel, and the fracture occurs by a ductile dimple rupture. However, the understanding of the underlying influence of different precipitates on the mechanical properties of the Fe-Ni-Al-Mn-based steels remains incomplete.

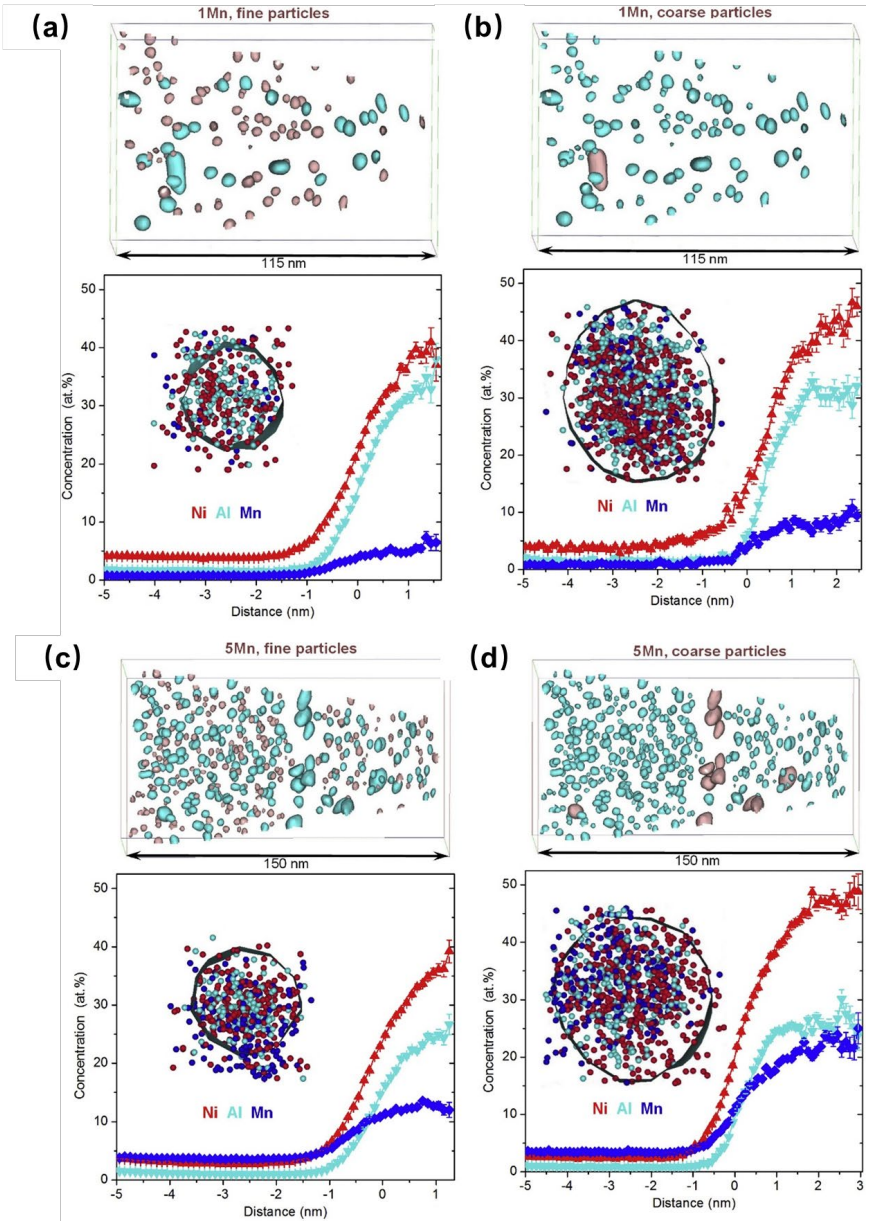

Fig. 4. APT showing morphology and composition of the precipitates in the Fe-5Ni-1Al-1Mn (1Mn) and Fe-5Ni-1Al-5Mn (5Mn) steels aged at 550 °C for 2 h: (a) fine particles, 1Mn steel, (b) coarse particles, 1Mn steel, (c) fine particles, 5Mn steel, and (d) coarse particles, 5Mn steel [30].

2.5 Mo-enriched precipitate

Mo-enriched precipitates are also an important type of strengthening phases in the maraging steels. Different kinds of Mo-enriched precipitates can be formed, such as Laves phase (Fe_2Mo), ω phase (Fe_7Mo_2), μ phase (Fe_7Mo_6), orthorhombic Ni_3Mo quasicrystalline R′ phase, and trigonal R phase, highly depending on the alloy composition and teat treatment [34-37]. Sha *et al.* [38] reported that the precipitation behavior of Mo-enriched precipitates is influenced by Ni_3Ti precipitates. They found that the ω phase was formed in the Ti-free steel; however, no ω phase was detected in the Ti-containing steel. Niu *et al.* [39] studied the synergistic effects of Mo and Ti on nanoscale precipitation in the steels strengthened by Ni_3Ti and Mo-enriched precipitates (Ti/Mo-steel). **Figure 5** shows the distribution of Ni_3Ti and Mo-enriched precipitates in the steel after aging for different times. The APT results indicate that in the early stage of precipitation, Mo is distributed in the core of the Ni_3Ti precipitates. As the precipitation proceeds, Mo atoms are rejected from the core of the Ni_3Ti precipitates to the interface. In addition, the Ni_3Ti/matrix interface provides a large number of nucleation sites for Mo-enriched precipitates, which leads to the heterogeneous precipitation of Mo-enrich precipitates. In addition, the Mo-enriched precipitates also influence the precipitation of Ni_3Ti. Andersson *et al.* [40] compared the precipitation behavior of high-Mo and low-Mo maraging stainless steels and found that the Mo-enriched phase slows down the coarsening rate of the $Ni_3(Ti,Al)$ precipitates due to its sluggish diffusion and growth.

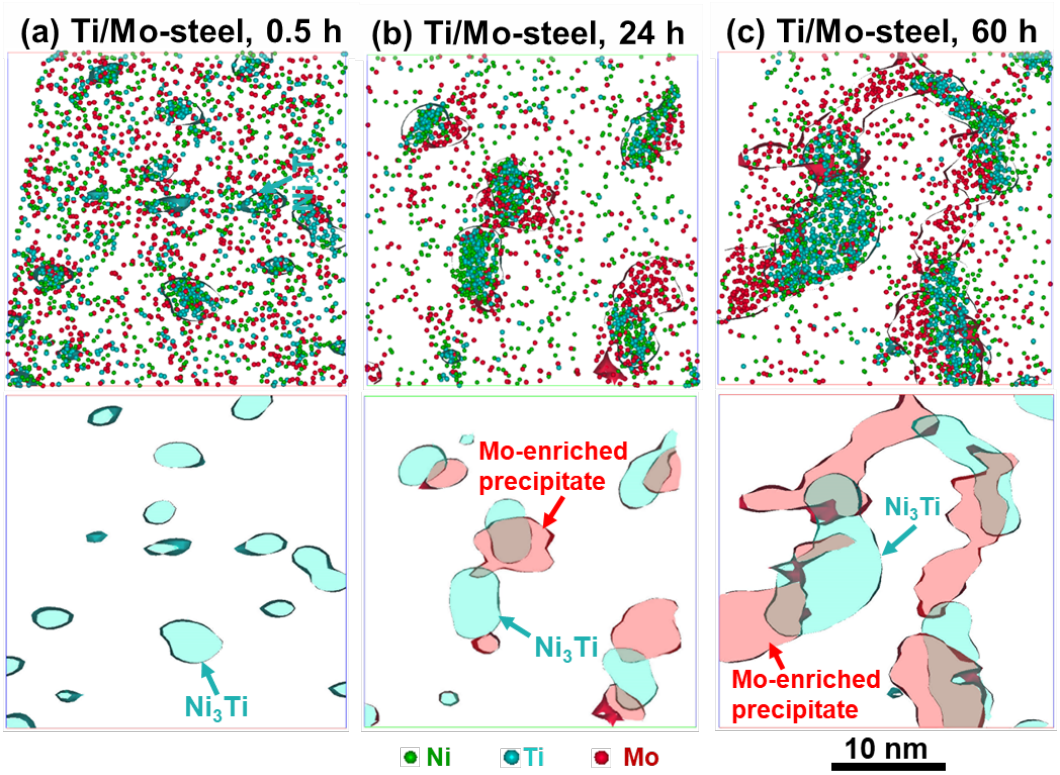

Figure 5. The distribution of Ni_3Ti and Mo-enriched precipitates in the Ti/Mo-steel after aging different times: (a) 0.5 h, (b) 24 h, and (c) 60 h [39].

3. Mechanical properties

To compare the strengthening effect of different types of precipitates, we summarize the yield strength increment induced by Ni_3Ti, NiAl, Cu, Ni_2AlMn, and Laves precipitates with a number density of 10^{24} m^{-3} in **Fig. 6**. It is evident that these precipitates have significantly different strengthening responses. For example, Ni_3Ti and NiAl precipitates induce a yield strength increment of 1200 and 1100 MPa, respectively [23,41]. The yield strength increment induced by the Laves, Cu and Ni_2AlMn precipitates are 500, 450, and 410 MPa, respectively [30,39,42]. However, improving strength often causes the decline of ductility and toughness, which is called the strength-ductility/toughness trade-off dilemma in structural materials. Materials scientists have tried to overcome this dilemma through the elaborate design of the alloys. For example, Floreen [43] addressed the grain boundary embrittlement in classical 18%Ni maraging steel by the addition of 2% Mo, which changed the deformation mode from intergranular to transgranular, substantially improving the tensile ductility. Liu *et al.* [44]

developed a new UHSS with a good combination of strength (2.4 GPa), ductility (~11%) and impact toughness (37 J/cm^2) based on the synergistic strengthening of high-density dislocations, massive NiAl nano-precipitates, strong segregations of elements (C, Mo, and Cr) on dislocations, and an ultrafine lath structure of martensite.

A small amount of retained and/or reverted austenite can improve the ductility and toughness by the transformation-induced plasticity (TRIP) effect. Millán *et al.* [32] designed a low-Ni TRIP maraging steel by controlling Mn additions, which achieves an ultimate tensile strength of 1 GPa and a total elongation of 15%. Niu *et al.* [45] reported an innovative strategy to accelerate the austenite reversion by Cu precipitation in maraging steels. The microstructure of the steels in the peak-aged condition characterized by TEM and APT is shown in **Fig. 7**. It can be seen that Cu, as an austenite-forming element, partitions in the reverted austenite, improving the driving force for the austenite formation. In addition, Cu precipitates were detected adjacent to the reverted austenite, indicating that the Cu precipitates could provide preferred nucleation sites for the austenite reversion. As a result, the nucleation of reverted austenite is drastically promoted. These steels strengthened by Cu precipitates and toughened by reverted austenite exhibit a good combination of strength (1330 MPa), ductility (15%) and impact toughness (58 J).

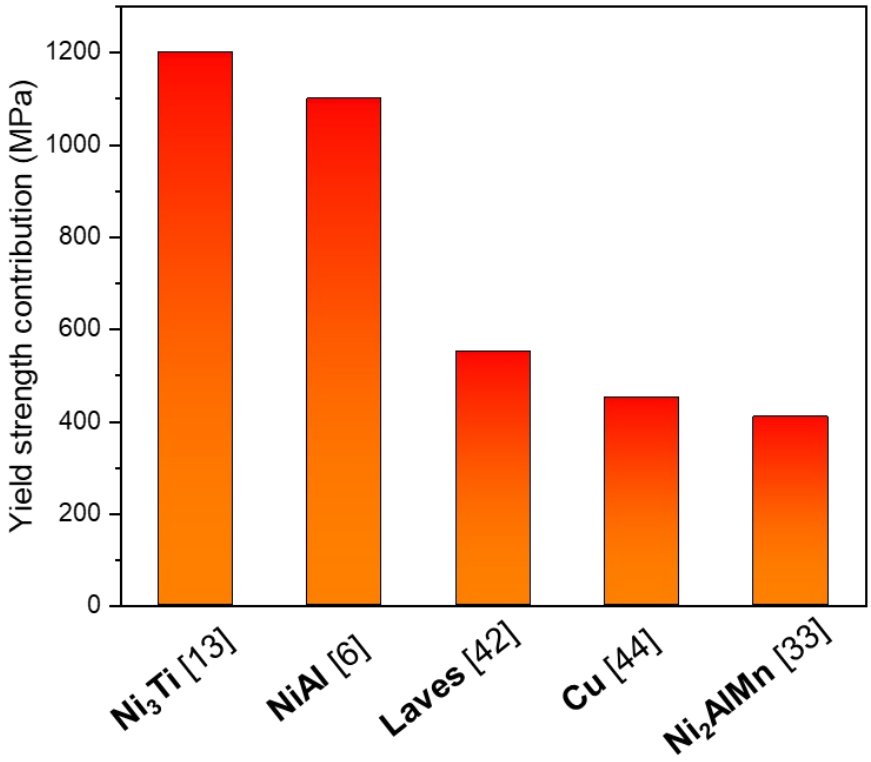

Figure 6. The yield strength contribution of steels given by different types of precipitates [23,30,39,41,42].

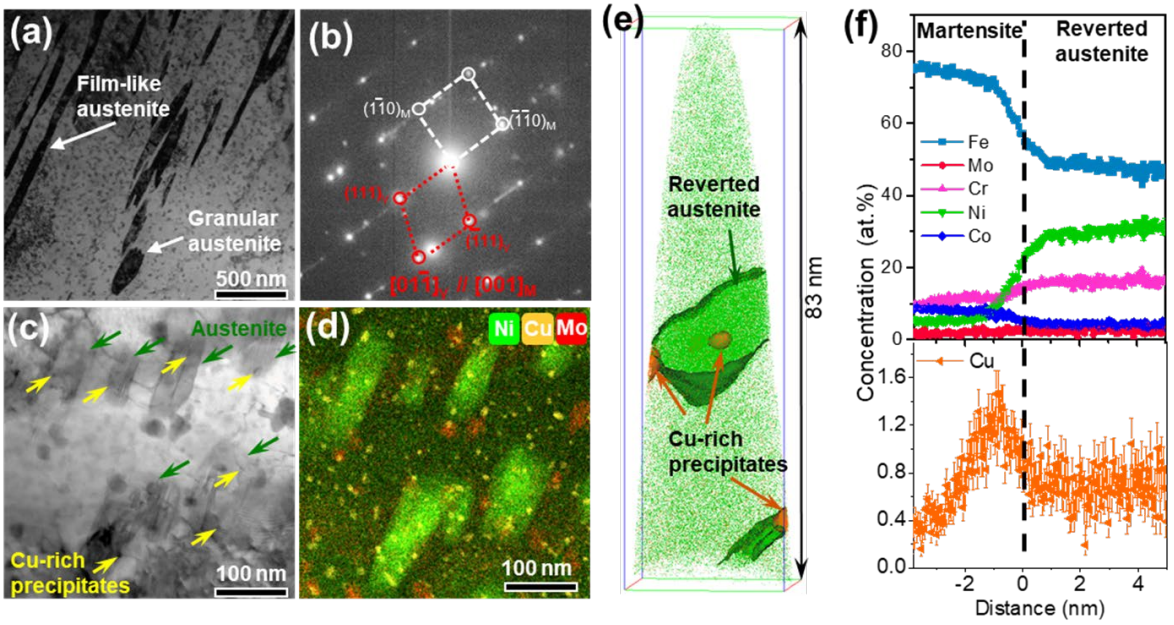

Figure 7. Microstructure of Cu-containing steel characterized by TEM and APT [45].

Nano-precipitation-strengthened steels also have a broad application prospect as heat-resistant materials. Especially, the NiAl-strengthened ferritic steels have low thermal

expansion, good thermal stability, and reasonable cost [46-49]. Intriguingly, the precipitate microstructure of NiAl-strengthened ferritic steels are similar to that of $L1_2$-γ'-strengthened Ni-based superalloys, which show outstanding creep resistance at elevated temperatures. However, due to the low lattice mismatch, the NiAl precipitates become soft with increased temperature and are not sufficiently strong to resist the dislocation climbing. Therefore, the creep strength of the NiAl-strengthened ferritic steels decrease sharply at elevated temperatures, especially above 700 ℃ [50]. Recently, it has been found that the NiAl-strengthened ferritic steels modified with Ti additions drastically improve the creep resistance of the ferritic steels at elevated temperatures, which develop hierarchical NiAl (B2)/Ni_2AlTi ($L2_1$) co-precipitates in the matrix. Rawlings *et al.* [47] compared the creep properties of the Fe-Cr-Ni-Al (FBB8) alloy with and without 2% Ti addition. The results show that the precipitation of $L2_1$ in the B2 precipitates increases the creep threshold stress from 69 to 179 MPa at 700 ℃, which is attributed to the fact that the co-precipitation of B2 and $L2_1$ enhances the elastic interaction strain fields with a large lattice mismatch. The lattice parameter mismatch between the $L2_1$ precipitates and bcc-matrix is larger than that between the B2 precipitates and bcc-matrix, which makes the B2/$L2_1$ co-precipitates more difficult for the matrix dislocations to bypass. In the shearing process, the B2/$L2_1$ co-precipitates hinder the dislocation movement by switching the preferential slip plane when they shear through the dual-phase precipitates. These results provide a novel strategy for developing new creep-resistant ferritic steels.

4. Corrosion and oxidation resistance

Although nano-precipitation-strengthened steels have been used successfully in the aerospace sector for decades. These materials, however, are susceptible to corrosion. They usually require a form of protection, particularly when used in aggressive environments, such as maritime climates. Currently, the most common solution is the electroplating of components with a sacrificial cadmium metal coat. While the inherent toxicity of cadmium metal and its corrosion products keeps them from being an ideal solution. Hence, tremendous efforts have been put forth to develop ultrahigh strength stainless steel by controlling Cr additions. An innate passive oxide film composed primarily of chromium oxide (Cr_2O_3) could be formed at

the stainless steel surface when exposed to the atmosphere, which is capable to replace existing alloys while eliminating the need for an additional coat and all of the associated processing, maintenance, and costs [51]. Jiang *et al.* [52] reported that the 00Cr13Ni7Co5Mo4W alloy has a breakdown potential of 230 mV with an annual corrosion rate of 1.5 μm/year, which is able to passivate readily even on exposure to seawater. However, they also found that the formation of Cr and Mo depletion zones around the Cr/Mo-rich R precipitates during aging resulted in the susceptibility to pitting corrosion. Tian *et al.* [51] studied the relative corrosion resistance of the high-Co maraging stainless steels, founding that the spinodal decomposition of Cr in the matrix makes the newly formed passive film unstable and uneven, which could be destroyed easily by the corrosive medium during the passivation process, thereby resulting in poor corrosion resistance. They also found that Co promoted the spinodal decomposition of Cr in the aging process, which deteriorated the corrosion resistance of the steel [53]. By reducing the Co content and increasing the Ti content, they developed a new class of maraging stainless steels with an ultimate tensile strength of 1.9 GPa and a high toughness of 77 $MPa \cdot m^{1/2}$ and superior corrosion resistance [54].

Cr is also added in UHSS to improve the oxidation resistance by forming an innate dense Cr_2O_3 oxide film. In addition, Al is added to the steels to form a protective Al_2O_3 layer, which could further improve the oxidation resistance, especially at temperatures of higher than 700 °C. Rawers and Mattlin [55] studied the oxidation resistance of Fe-12Ni-7Cr steels with different additions of Al (0 to 6 wt.%) at 800-1000 °C. It was found that the remarkable improvement of the oxidation resistance was due to the formation of a protective Al_2O_3 layer, which formed over the Cr_2O_3 layer when the Al content was between 3 and 4.5 wt.%. Basuki *et al.* [56] studied the oxidation behavior of a 69.5Fe-14Ni-7.5Cr-9Al (wt.%) steel at 800-1000 °C. They found that the oxidation rate increased with temperature and followed a logarithmic equation, suggesting that the oxide layer was very thin and protective.

5. Welding properties

Traditional high-strength carbon steels have poor weldability, because a brittle heat-affected zone (HAZ) is usually formed near the weld, whereas the nano-precipitation-

strengthened steels with an ultra-low carbon content can possibly solve the problem. Numerous studies on these materials have demonstrated that the HAZ softens significantly due to the dissolution of the nano-precipitates during welding [57]. Currently, researchers have found that the re-precipitation of nanoparticles can be achieved by two commonly used methods to restore the mechanical properties. One is by appropriate post-weld heat treatment (PWHT). For example, Jiao *et al.* [58] studied the effect of welding and PWHT on the microstructure and mechanical properties of the NiAl/Cu co-precipitates strengthened steels. The APT microstructure of the fusion zone (FZ) under different conditions is shown in **Fig. 8**. The APT analysis shows that a supersaturated solid solution was formed in the FZ after welding, which is due to the dissolution of all pre-existing nanoparticles during the welding process. The PWHT at 550 °C leads to a great recovery of strength and ductility, because the high number densities of nanoscale NiAl and Cu particles are re-precipitated. While the PWHT at 600 °C leads to the re-precipitation of coarse-scale nanoparticles and the formation of a small amount of reverted austenite, resulting in a great recovery of strength and ductility. However, the cost of PWHT is high and not suitable for large-scale welding or field maintenance. Therefore, the multi-pass welding technique provides another method to re-precipitate nanoparticles. Yu *et al.* [59] investigated the effect of multiple welding thermal cycles on the Cu precipitation in a low-carbon martensitic steel. The APT and hardness measurements demonstrated that the precipitates dissolved during the primary high-temperature thermal cycles, and they re-formed after the secondary medium-temperature thermal cycles. Robert *et. al* [60] studied the PH 13-8 Mo and PH 17-4 subjected to a series of short isothermal holds at various temperatures through welding thermal cycles. They found that the re-precipitation can be restored during the subsequent multi-pass welding thermal cycles. These findings indicate that controlling the welding technique may be a viable method to optimize mechanical properties of welded high-strength steels.

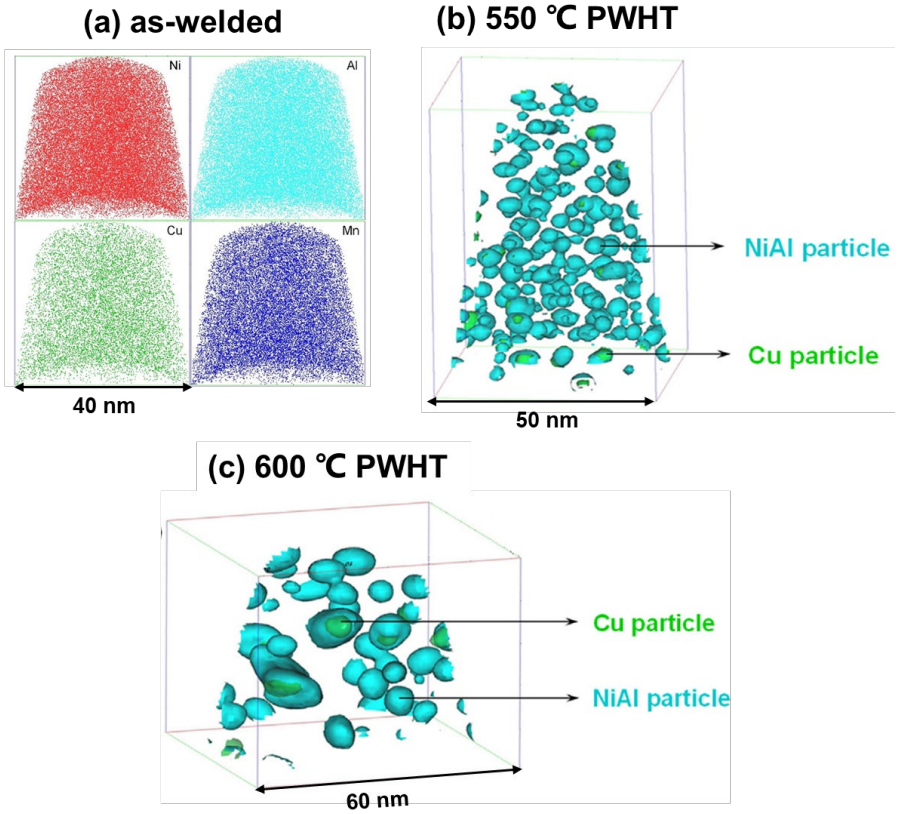

Figure 8. APT characterization of the fusion zone in the different conditions: (a) as-welded, (b) PWHT at 550 ℃ and (d) PWHT at 600 ℃ [58].

6. Additive manufacturing of nano-precipitation-strengthened steels

Metal additive manufacturing (AM) is a subversive manufacturing technology that uses a high-energy heating source and uses powders, wires or plates as feeding materials to manufacture complex engineering parts layer by layer. Maraging steels and PH stainless steels are two classes of nano-precipitation-strengthened steels that have been widely studied and are suitable for production through AM. Roberts *et al.* [60] compared the mechanical properties and microstructure of AM 15-5 PH stainless steel with a wrought 15-5 PH stainless steel. The yield strength of the horizontally constructed samples increased by about 10%, whereas that of the vertically constructed samples decreased by about 6%. Regardless of the direction of construction, the ultimate tensile strength increased by a similar amplitude compared with the forged samples (approximately 11% for the horizontal construction and 12% for the vertical construction). The Charpy impact energy of the AM 15-5 PH stainless steel is ~11 J/cm^2, which

is similar to that of wrought samples (9.4 ~ 18.6 J/cm^2). Lass *et al.* [61] analyzed the mechanical properties of AM 17–4 PH samples under different post-build heat treatment conditions and compared the results with the wrought samples under the same heat-treatment conditions. After post-build solution and aging treatment, the yield strength of the AM 17–4 PH samples reaches a 90% yield strength of the wrought samples. Post-build heat treatments are also adopted to maraging steels to improve their mechanical properties. Kempen *et al.* [62] reported that an 18Ni 300 maraging steel by laser powder bed fusion (LPBF) has an ultimate tensile strength of 2217 MPa after solution and aging treatments, which is even higher than that of the forged sample (2210 MPa). It was also found that the LPBF maraging steel has the best tribological properties than the cast steel [63]. Therefore, by reasonably selecting the processing parameters and manufacturing strategies, AM maraging steels can have comparable or even better mechanical properties than the steels fabricated through conventional ways. In addition, Kürnsteiner *et al.* [64] developed a Fe-19Ni-5Ti maraging steel with a hierarchical structure by AM using digital control of the intrinsic heat treatment (IHT) sequences related to the layered manufacturing technology. This steel is hardened *in situ* by Ni_3Ti nano-precipitation, and the martensitic matrix is also formed *in situ*, starting from the readily accessible temperature of 200 ℃. Local control of nano-precipitation and martensitic transformation in the manufacturing process leads to complex microstructure grades spanning multiple length scales, from approximately 100 μm thick layers to nano-scale precipitates. This material is composed of soft and hard layers alternately, which achieves a tensile strength of 1300 MPa and an elongation of 10%, showing excellent mechanical properties comparable to the ancient Damascus steel. The strategy of *in-situ* precipitation strengthening and local microstructure control provides a new avenue for developing advanced nano-precipitation strengthened steels through AM processes.

7. Future perspectives

In view of their ultra-high strength and good toughness and ductility, nano-precipitation-strengthened steels have a broad application prospect in the future aviation, aerospace, marine, and nuclear industries. To further speed up the development of new UHSSs and promote their

industrial applications, future efforts should be focused on the critical issues of these materials, including hydrogen embrittlement, stress corrosion, and thermal stability.

7.1 Hydrogen embrittlement

Steels are more sensitive to hydrogen embrittlement (HE) with the increase of strength grade. Especially, when polluting or corrosive gas components and hydrogen acting on the steels together with stresses, the crack initiation becomes easy and gradually expands, leading to the macroscale cracking. Diffusible hydrogen is the main factor causing the plastic loss of steels, and any measures to reduce the mobility of diffusible hydrogen can improve the sensitive resistance of materials to HE. A strong hydrogen trap can improve the absorption of supersaturated hydrogen in steels, decreasing the concentration of diffusible hydrogen. Notably, in nano-precipitation-strengthened steels, a large number of dispersed precipitates and reversed austenite precipitates can serve as hydrogen traps. Studies show that carbides are typical "benign hydrogen traps" in steels, which can effectively improve the hydrogen embrittlement sensitivity of steels [65]. Recently, Li *et al.* [66] compared the hydrogen embrittlement behaviors of PH 17-4 and PH 13-8Mo steels by hydrogen permeation tests and slow strain rate tensile tests. The results show that the incoherent Cu-rich precipitates in the PH 17-4 steel have higher ability to capture hydrogen atoms than the coherent NiAl precipitates in the PH 13-8Mo steel. The findings are consistent with the observation nathat the PH 13-8Mo steel has lower apparent hydrogen solubility and higher apparent hydrogen diffusion coefficient than the PH 17-4 steel. In addition, some studies suggested that the dislocation core on the coherent interface and the lattice near the dislocation core with a small distortion are weak hydrogen traps, and the de-trapping energy of non-coherent precipitates is higher than that of coherent precipitates [67]. The fundamental understanding of the role of different types of nano-precipitates as hydrogen traps and their effects on the HE needs to be further studied.

7.2 Stress and pitting corrosion

Stress corrosion cracking is one of the main forms of sudden damage accidents of key load-bearing components of aircraft in service. Most landing gears are failed due to the stress

corrosion or fatigue crack propagation. The stress corrosion occurs in almost all commonly used steels and alloys. It is of great scientific value and practical significance to understand the mechanism controlling the stress corrosion cracking and the key factors governing the stress corrosion. Many stress corrosion cracks originate from pits. During the aging process, the microstructure of the martensitic matrix becomes non-uniform, and the passive film near the precipitates is weaker than the matrix, which is easy to be destructed by the invasion of Cl^-, thereby causing the pitting corrosion. Luo *et al.* [68] studied the microstructure and electrochemical behavior of a 15-5 PH stainless steel by APT. Cu-rich precipitates were detected after aging for 15 min. After aging 4 h, nano-scale (Cu,Nb)-rich carbides were detected. The electrochemical studies showed that the pitting corrosion increases with increasing aging time, which is due to the formation of Cr-depleted zones around the precipitates. In addition, the decrease of Cr/Fe ratio, the increase of hydroxides, and the dehydration effect in the passive films after the long-term aging decrease the resistance to pitting corrosion. The stress and pitting corrosion of UHSSs can be affected by many factors. It is necessary to establish multi-scale models of stress and pitting corrosion in UHSSs and develop useful techniques to improve their corrosion resistance.

7.3 Thermal stability

Thermal stability of nanoparticles is a very important factor that has to be taken into consideration when the nano-precipitates-strengthened steels are used at elevated temperatures. Because after a long-term exposure at elevated temperatures, the precipitates coarsen and lose the strengthening effect. Interestingly, Sun et al. [49] reported a new class of NiAl-precipitate-strengthened ferritic steels, the strength of which can be remained after exposure at 700 ℃ for 500 h. In addition, previous studies indicate that the thermal stability of this kind of steels could be improved by the B2-NiAl/ $L2_1$-Ni_2TiAl co-precipitates. This is due to the good microstructural stability of the $L2_1$-Ni_2TiAl phase at high temperatures. Generally, the coarsening of precipitates is related to the interfacial energy of the precipitates as well as the solubility limit and diffusion rate of solute elements. However, Ni_2TiAl is a very brittle phase, which causes a low ductility of the materials at room temperature, thus limiting their industrial

applications. Hence, it is of both scientific and technological importance develop advanced nano-precipitation-strengthened steels with high strength and stability at high temperatures and good ductility at low temperatures.

8. Summary

This chapter highlights the recent advances in the steels strengthened by various precipitates, including Ni_3Ti, NiAl, Cu, Ni_2AlMn, and Mo-enriched precipitates. This class of steels show excellent mechanical properties at room and high temperatures as well as good welding and corrosion performance, which make them promising candidates for technological applications. The synergistic alloying effects on nanoscale precipitation and mechanical properties of these matrials are discussed, and the the co-precipitation of NiAl/Cu, NiAl/Ni2AlMn, NiAl/Ni_2AlTi, Ni_3Ti/Mo-enriched co-precipitates in steels is presented. Future efforts should be focused on understanding and improving the hydrogen embrittlement sensitivity, stress corrosion resistance, and thermal stability of these steels.

Acknowledgement

This research was supported by the National Natural Science Foundation of China (52171162), Shenzhen Science and Technology Program (JCYJ20210324142203009), Research Grants Council of Hong Kong (ECS 25202719, GRF 15227121, C1017-21GF, and C1020-21GF), and Research Institute for Advanced Manufacturing at PolyU (P0041364).

References

[1] S.K. Banerji, C.J. McMahon, H.C. Feng, Intergranular fracture in 4340-type steels: Effects of impurities and hydrogen, Metall. Trans. A 9(2) (1978) 237-247.
[2] E.J. Czyryca, Advances in high strength steel technology for naval hull construction, Key Engineering Materials 84-85 (1993) 491-520.
[3] G.E. Pellissier, Effects of microstructure on the fracture toughness of ultrahigh-strength steels, Eng. Fract. Mech. 1(1) (1968) 55-75.
[4] H.-W. Yen, P.-Y. Chen, C.-Y. Huang, J.-R. Yang, Interphase precipitation of nanometer-sized carbides in a titanium–molybdenum-bearing low-carbon steel, Acta Mater. 59(16) (2011) 6264-6274.
[5] S.B.P. J., W.C. M., Crystallography and substructure of lath martensite formed in carbon steels, Metallography 16 (1983) 199-227

[6] R. Ayer, P.M. Machmeier, Microstructural basis for the effect of chromium on the strength and toughness of AF1410-based high performance steels, Metallurgical and Materials Transactions A 27(9) (1996) 2510-2517.
[7] M.R. Ahmadi, E. Povoden-Karadeniz, K.I. Oksuz, A. Falahati, E. Kozeschnik, A model for precipitation strengthening in multi-particle systems, Comput. Mater. Sci. 91 (2014) 173-186.
[8] J.S. Wang, M.D. Mulholland, G.B. Olson, D.N. Seidman, Prediction of the yield strength of a secondary-hardening steel, Acta Mater. 61(13) (2013) 4939-4952.
[9] H. Leitner, R. Schnitzer, M. Schober, S. Zinner, Precipitate modification in PH13-8 Mo type maraging steel, Acta Mater. 59(12) (2011) 5012-5022.
[10] F.J. Arrieta Blanco, M.P. Saavedra Vallejo, J. Tunon Fernandez, G. Marin Hernandez, M. Aguirre Jaca, [Efficacy of ketoconazole in the treatment of systemic candidiasis with pulmonary involvement], Rev. Clin. Esp. 182(2) (1988) 114.
[11] Z.W. Zhang, C.T. Liu, S. Guo, J.L. Cheng, G. Chen, T. Fujita, M.W. Chen, Y.-W. Chung, S. Vaynman, M.E. Fine, B.A. Chin, Boron effects on the ductility of a nano-cluster-strengthened ferritic steel, Mater. Sci. Eng., A 528(3) (2011) 855-859.
[12] Q.-D. Liu, J.-F. Gu, C.-W. Li, Regulation of Cu precipitation by intercritical tempering in a HSLA steel, J. Mater. Res. 29(8) (2014) 950-958.
[13] Vijay K. Vasudevan, Sung J. Kim, C.M. Wayman, Precipitation reactions and strengthening behavior in 18 wt pct nickel maraging steels, Metall. Trans. A 21A (1990) 2655-2668.
[14] M.S. Kim, Y.U. Heo, H.C. Lee, The Grain Boundary Embrittlement and De-Embrittlement Mechanism in Age Hardenable Fe-Ni-Ti Steels, Solid State Phenom. 118 (2006) 469-474.
[15] N.H. Heo, Grain boundary segregation and intergranular fracture in Ferrite containing Mo, Si or Al, Met. Mater. 2(1) (1996) 49-64.
[16] N.H. Heo, J.G. Na, Effect of alloying elements on fracture behavior of Fe-18Ni-2Ti-(8Co) alloys, Met. Mater. 3(2) (1997) 125-129.
[17] N.H. Heo, L.H. C., Role of Chromium on Mechanical Properties of Fe-Mn-Ni-Mo-Ti Maraging Steels, Met. Mater. 1 (1995) 77-83.
[18] N.Q. Vo, C.H. Liebscher, M.J.S. Rawlings, M. Asta, D.C. Dunand, Creep properties and microstructure of a precipitation-strengthened ferritic Fe–Al–Ni–Cr alloy, Acta Mater. 71 (2014) 89-99.
[19] M. Kapoor, Design and Development of bcc-Cu- and B2 NiAl-PrecipitationStrengthened Ferritic Steel, (2013).
[20] Z.B. Jiao, J.H. Luan, Z.W. Zhang, M.K. Miller, C.T. Liu, High-strength steels hardened mainly by nanoscale NiAl precipitates, Scripta Mater. 87 (2014) 45-48.
[21] Q. Shen, H. Chen, W. Liu, Effect of Cu on Nanoscale Precipitation Evolution and Mechanical Properties of a Fe-NiAl Alloy, Microsc. Microanal. 23(2) (2017) 350-359.
[22] K. Soeno, M. Tuchiya, Precipitation hardening and magnetic properties of Fe-Ni-Al, Fe-Ni-Ti and Fe-Ni-Co-Mo maraging steels, ISIJ Int. 60(9) (1973) 105-114.
[23] S. Jiang, H. Wang, Y. Wu, X. Liu, H. Chen, M. Yao, B. Gault, D. Ponge, D. Raabe, A. Hirata, M. Chen, Y. Wang, Z. Lu, Ultrastrong steel via minimal lattice misfit and high-density nanoprecipitation, Nature 544(7651) (2017) 460-464.
[24] Y.U. Heo, Y.K. Kim, J.S. Kim, J.K. Kim, Phase transformation of Cu precipitates from

bcc to fcc in Fe–3Si–2Cu alloy, Acta Mater. 61(2) (2013) 519-528.
[25] G. Han, Z.J. Xie, Z.Y. Li, B. Lei, C.J. Shang, R.D.K. Misra, Evolution of crystal structure of Cu precipitates in a low carbon steel, Mater. Design. 135 (2017) 92-101.
[26] M. Kapoor, D. Isheim, G. Ghosh, S. Vaynman, M.E. Fine, Y.-W. Chung, Aging characteristics and mechanical properties of 1600MPa body-centered cubic Cu and B2-NiAl precipitation-strengthened ferritic steel, Acta Mater. 73 (2014) 56-74.
[27] Z.B. Jiao, J.H. Luan, M.K. Miller, Y.W. Chung, C.T. Liu, Co-precipitation of nanoscale particles in steels with ultra-high strength for a new era, Mater. Today 20(3) (2017) 142-154.
[28] R. Schnitzer, M. Schober, S. Zinner, H. Leitner, Effect of Cu on the evolution of precipitation in an Fe–Cr–Ni–Al–Ti maraging steel, Acta Mater. 58(10) (2010) 3733-3741.
[29] Y.U. Heo, M. Takeguchi, K. Furuya, H.C. Lee, Discontinuous coarsening behavior of Ni(2)MnAl intermetallic compound during isothermal aging treatment of Fe-Mn-Ni-Al alloys, J Electron Microsc (Tokyo) 59 Suppl 1 (2010) S135-40.
[30] Z.B. Jiao, J.H. Luan, M.K. Miller, C.Y. Yu, Y. Liu, C.T. Liu, Precipitate transformation from NiAl-type to Ni_2AlMn-type and its influence on the mechanical properties of high-strength steels, Acta Mater. 110 (2016) 31-43.
[31] J. Millán, S. Sandlöbes, A. Al-Zubi, T. Hickel, P. Choi, J. Neugebauer, D. Ponge, D. Raabe, Designing Heusler nanoprecipitates by elastic misfit stabilization in Fe–Mn maraging steels, Acta Mater. 76 (2014) 94-105.
[32] J. Millán, D. Ponge, D. Raabe, P. Choi, O. Dmitrieva, Characterization of Nano-Sized Precipitates in a Mn-Based Lean Maraging Steel by Atom Probe Tomography, Steel Res. Int. 82(2) (2011) 137-145.
[33] Y.-U. Heo, H.-C. Lee, Precipitation and fracture behaviour of Fe–Mn–Ni–Al alloys, Philos. Mag. 93(36) (2013) 4519-4531.
[34] M. Niu, G. Zhou, W. Wang, M.B. Shahzad, Y. Shan, K. Yang, Precipitate evolution and strengthening behavior during aging process in a 2.5 GPa grade maraging steel, Acta Mater. 179 (2019) 296-307.
[35] W. Sha, A. Cerezo, G.D.W. Smith, Phase chemistry and precipitation reactions in maraging steels: part I. Introduction and study of Co-containing C-300 steel, Metall. Trans. A 24A (1993).
[36] Krystyna Stiller, Frederic Danoix, M. Ha¨ttestrand, Mo precipitation in a 12Cr-9Ni-4Mo-2Cu maraging steel, Materials Science and Engineering A 250 (1998) 22-26.
[37] A. Verdiere, C. Hofer, S. De Waele, V. Bliznuk, S. Primig, S. Cottenier, M.D. Tran, B. Pennings, L.A.I. Kestens, R.H. Petrov, Precipitation in simultaneously nitrided and aged Mo-containing maraging steel, Mater. Charact. 131 (2017) 21-30.
[38] W. Sha, A. Cerezo, G.D.W. Smith, Phase chemistry and precipitation reactions in maraging steels: part IV. discussion and conclusions, Metall. Trans. A 24A (1993) 1251.
[39] M.C. Niu, L.C. Yin, K. Yang, J.H. Luan, W. Wang, Z.B. Jiao, Synergistic alloying effects on nanoscale precipitation and mechanical properties of ultrahigh-strength steels strengthened by Ni3Ti, Mo-enriched, and Cr-rich co-precipitates, Acta Mater. 209 (2021) 116788.
[40] M. Andersson, K. Stiller, M. Hättestrand, Comparison of early stages of precipitation in Mo-rich and Mo-poor maraging stainless steels, Surf. Interface. Anal. 39(2-3) (2007) 195-

200.
[41] U.K. Viswanathan, G.K. Dey, M.K. Asundi, Precipitation Hardening in 350 Grade Maraging Steel, Metallurgical and Materials Transactions A 24(11) (1993) 2429-2442.
[42] H.J. Kong, C. Xu, C.C. Bu, C. Da, J.H. Luan, Z.B. Jiao, G. Chen, C.T. Liu, Hardening mechanisms and impact toughening of a high-strength steel containing low Ni and Cu additions, Acta Mater. 172 (2019) 150-160.
[43] S. Floreen, The physical metallurgy of maraging steels, Metallurgical Reviews 13(1) (2013) 115-128.
[44] T. Liu, Z. Cao, H. Wang, G. Wu, J. Jin, W. Cao, A new 2.4 GPa extra-high strength steel with good ductility and high toughness designed by synergistic strengthening of nano-particles and high-density dislocations, Scripta Mater. 178 (2020) 285-289.
[45] M.C. Niu, K. Yang, J.H. Luan, W. Wang, Z.B. Jiao, Cu-assisted austenite reversion and enhanced TRIP effect in maraging stainless steels, J. Mater. Sci. Technol. 104 (2022) 52-58.
[46] G. Song, Z. Sun, J.D. Poplawsky, Y. Gao, P.K. Liaw, Microstructural evolution of single Ni2TiAl or hierarchical NiAl/Ni2TiAl precipitates in Fe-Ni-Al-Cr-Ti ferritic alloys during thermal treatment for elevated-temperature applications, Acta Mater. 127 (2017) 1-16.
[47] M.J.S. Rawlings, C.H. Liebscher, M. Asta, D.C. Dunand, Effect of titanium additions upon microstructure and properties of precipitation-strengthened Fe-Ni-Al-Cr ferritic alloys, Acta Mater. 128 (2017) 103-112.
[48] S.-I. Baik, S.-Y. Wang, P.K. Liaw, D.C. Dunand, Increasing the creep resistance of Fe-Ni-Al-Cr superalloys via Ti additions by optimizing the B2/L21 ratio in composite nano-precipitates, Acta Mater. 157 (2018) 142-154.
[49] L. Sun, T.H. Simm, T.L. Martin, S. McAdam, D.R. Galvin, K.M. Perkins, P.A.J. Bagot, M.P. Moody, S.W. Ooi, P. Hill, M.J. Rawson, H.K.D.H. Bhadeshia, A novel ultra-high strength maraging steel with balanced ductility and creep resistance achieved by nanoscale β-NiAl and Laves phase precipitates, Acta Mater. 149 (2018) 285-301.
[50] Z.K. Teng, M.K. Miller, G. Ghosh, C.T. Liu, S. Huang, K.F. Russell, M.E. Fine, P.K. Liaw, Characterization of nanoscale NiAl-type precipitates in a ferritic steel by electron microscopy and atom probe tomography, Scripta Mater. 63(1) (2010) 61-64.
[51] J.-L. Tian, W. Wang, M.B. Shahzad, W. Yan, Y.-Y. Shan, Z.-H. Jiang, K. Yang, Corrosion Resistance of Co-containing Maraging Stainless Steel, Acta Metallurgica Sinica (English Letters) 31(8) (2018) 785-797.
[52] Y. Jiang, Y.Y. Ai, Q.T. Wang, Study on Corrosion Resistance of 00Cr13Ni7Co5Mo4W Maraging Stainless Steel in Seawater, Applied Mechanics and Materials 274 (2013) 402-405.
[53] J. Tian, W. Wang, L. Yin, W. Yan, Y. Shan, K. Yang, Three dimensional atom probe and first-principles studies on spinodal decomposition of Cr in a Co-alloyed maraging stainless steel, Scripta Mater. 121 (2016) 37-41.
[54] J. Tian, W. Wang, M. Babar Shahzad, W. Yan, Y. Shan, Z. Jiang, K. Yang, A New Maraging Stainless Steel with Excellent Strength-Toughness-Corrosion Synergy, Materials (Basel) 10(11) (2017).
[55] J.C. Rawers, E.M. Mattlin, Oxidation of Fe-7Cr-12Ni-(0-6)Al-(0-7)Si alloys, Metall. Trans. A 18(10) (1987) 1805-1812.

[56] E.A. Basuki, D.C. Nababan, F. Muhammad, A.A. Korda, D.H. Prajitno, Isothermal Oxidation Behaviour of 69.5Fe-14Ni-9Al-7.5Cr Alloy at High Temperatures, International Journal of Corrosion 2019 (2019) 1-8.
[57] J.R. Joshi, M. Potta, K. Adepu, M.R. Gankidi, R.K. Katta, Influence of Welding Techniques on Heat Affected Zone Softening of Dissimilar Metal Maraging Steel and High Strength Low Alloy Steel Gas Tungsten Arc Weldments, T. Indian I. Metals. 70(1) (2016) 69-81.
[58] Z.B. Jiao, J.H. Luan, W. Guo, J.D. Poplawsky, C.T. Liu, Effects of welding and post-weld heat treatments on nanoscale precipitation and mechanical properties of an ultra-high strength steel hardened by NiAl and Cu nanoparticles, Acta Mater. 120 (2016) 216-227.
[59] X. Yu, J.L. Caron, S.S. Babu, J.C. Lippold, D. Isheim, D.N. Seidman, Strength Recovery in a High-Strength Steel During Multiple Weld Thermal Simulations, Metallurgical and Materials Transactions A 42(12) (2011) 3669-3679.
[60] D. Roberts, Y. Zhang, I. Charit, J. Zhang, A comparative study of microstructure and high-temperature mechanical properties of 15-5 PH stainless steel processed via additive manufacturing and traditional manufacturing, Progress in Additive Manufacturing 3(3) (2018) 183-190.
[61] E.A. Lass, M.R. Stoudt, M.E. Williams, Additively Manufactured Nitrogen-Atomized 17-4 PH Stainless Steel with Mechanical Properties Comparable to Wrought, Metallurgical and Materials Transactions A 50(4) (2019) 1619-1624.
[62] K. Kempen, E. Yasa, L. Thijs, J.P. Kruth, J. Van Humbeeck, Microstructure and mechanical properties of Selective Laser Melted 18Ni-300 steel, Physics Procedia 12 (2011) 255-263.
[63] S. Yin, C. Chen, X. Yan, X. Feng, R. Jenkins, P. O'Reilly, M. Liu, H. Li, R. Lupoi, The influence of aging temperature and aging time on the mechanical and tribological properties of selective laser melted maraging 18Ni-300 steel, Additive Manufacturing 22 (2018) 592-600.
[64] P. Kurnsteiner, M.B. Wilms, A. Weisheit, B. Gault, E.A. Jagle, D. Raabe, High-strength Damascus steel by additive manufacturing, Nature 582(7813) (2020) 515-519.
[65] Y.S. Chen, H. Lu, J. Liang, A. Rosenthal, H. Liu, G. Sneddon, I. McCarroll, Z. Zhao, W. Li, A. Guo, J.M. Cairney, Observation of hydrogen trapping at dislocations, grain boundaries, and precipitates, Science 367(6474) (2020) 171-175.
[66] X. Li, J. Zhang, Q. Fu, E. Akiyama, X. Song, S. Shen, Q. Li, Hydrogen embrittlement of high strength steam turbine last stage blade steels: Comparison between PH17-4 steel and PH13-8Mo steel, Mater. Sci. Eng., A 742 (2019) 353-363.
[67] T. Depover, D. Pérez Escobar, E. Wallaert, Z. Zermout, K. Verbeken, Effect of hydrogen charging on the mechanical properties of advanced high strength steels, Int. J. Hydrogen. Energ 39(9) (2014) 4647-4656.
[68] H. Luo, Q. Yu, C. Dong, G. Sha, Z. Liu, J. Liang, L. Wang, G. Han, X. Li, Influence of the aging time on the microstructure and electrochemical behaviour of a 15-5PH ultra-high strength stainless steel, Corros. Sci. 139 (2018) 185-196.